JME

Journal of Mining & Environment,
Vol.6, No.2, 2015, 205-224.

Feasibility study of underground salt caverns in Western Newfoundland: experimental and finite element investigation of creep-induced damage

A. Ghasemloonia[1*] and S.D. Butt[2]

1. Postdoctoral Fellow, Subsurface Imaging Technology, St. John's, Newfoundland, Canada
2. Professor, Faculty of Engineering, Memorial University, St. John's, Newfoundland, Canada

Received 20 October 2014; received in revised form 6 June 2015; accepted 6 June 2015
**Corresponding author: a.ghasemloonia@mun.ca (A. Ghasemloonia).*

Abstract
Underground caverns in rock salt deposits are the most secure disposal method and a type of gas-storing facility. Gas storage plays a vital role in ensuring that a strategic relationship is secured between an established energy infrastructure provider and a midstream energy company. The Fischells Brook area is a pillow-shaped body of salts located in the St. George's Bay area of southwest Newfoundland, which has three layers of salt beds, and is capable of excavating caverns for the storage purposes. The development of cavern facilities requires the stability analysis through numerical models and experimental facilities. This work was motivated to examine the engineering feasibility of the salt cavern characteristics in this area, and to investigate its stability under creep behavior. An experimental test facility was developed to investigate the constitutive parameters governing the creep of rock salt, and the constitutive parameters were implemented into a developed finite element model to investigate the stability of the cavern over a 5-year period. Also a stress-based dilatancy failure envelope was developed to interpret the results of the numerical model, and to conduct sensitivity analyses for different design scenarios. The design recommendations developed in this study will be implemented as a key part of an engineering feasibility study for underground caverns in salt deposits in western Newfoundland.

Keywords*: Salt Cavern, Steady-State Creep Model, Dilatancy Envelope, FEM, Uniaxial Creep Test, Cavern Closure.*

1. Introduction

Salt rock due to low permeability and high ductility is an ideal material for the storage of underground natural gas, hydrocarbons, and radioactive wastes. Salt rock storage is usually produced by the dissolution process, and it facilitates higher pressure storage than surface storages. The land area required, less sensitivity to ambient excitations, and a lower dissolution cost compared to excavation are other advantages of the underground salt caverns. One of the critical design issues of the underground salt caverns is the time-dependent closure of the cavern due to the creep behavior of the salt. A salt rock displays a different time-dependent behavior from a solution-precipitation creep to the dislocation process, steady-state micro-cracking, strain weakening, and plastic viscous deformation, depending on the stress and temperature conditions [1]. At the engineering stress and temperature conditions under the ground, a salt rock exhibits a steady-state creep behavior. The creep behavior is induced by the shear stress around the cavern, which is the result of the difference between the cavern inside pressure and the in situ stress in the surrounding salt. Damage progresses with the progress of the creep, and causes the micro-fracturing and spalling of the cavern roof, and, finally, failure of the casing seat. Therefore, the time-dependent creep behavior of the salt cavern must be investigated, and the geometrical and operational parameters of the cavern are required to be developed by modeling this phenomenon.

In order to investigate the creep behavior of the salt, the constitutive model of the rock salt must be established and implemented into numerical models to study the creep behavior of the cavern under a prescribed pressure over a long time period. The creep behavior of a salt rock can be divided into three major stages: transient, steady-state, and tertiary. The steady-state creep behavior is the dominant type of behavior in the underground salt cavern, and numerous empirical models have been developed to model this behavior. The power law creep relation is the most accepted model used in the creep studies on the salt, and accounts for the principal stress differences, deviatoric stress, and temperature effects. The creep rate in the steady-state is constant, and the creep deformation is irreversible. Further discussion on the different creep behaviors of the salt can be found in the literature review section. The power law model has coefficients and constants, which should be investigated by experiments to develop the model for any particular type of rock salt.

The engineering creep tests for salts are usually carried out to develop the quantitative constitutive law which is implemented into numerical models to design a cavern. Three types of tests are common for the creep study of the salt: constant stress test, constant strain rate test, and relaxation test. Among these three tests, constant stress tests are ideal for determining the steady-state creep behavior of the salt, which is useful for the numerical modeling of a salt rock cavern over a long period of time. This test can be done in configurations such as the uniaxial and triaxial compressions. The applied stress value has been suggested to be approximately 60% of the UCS tests to precisely predict the creep behavior. The creep test results obtained are normally used to calibrate the standard creep models, which can then be used for the engineering analysis, design, and modelling. The calibration is based on the steady-state strain rate developed from the creep tests. In this investigation, a hydraulic frame actuator was developed to achieve the target stress level. Multi-staged constant stress tests were selected based on the stress levels that represented the depths of the Fischells Brook deposit. Also, the UCS tests were conducted to investigate the strength of the overlying formations.

Numerical modeling is the most efficient and cost-effective tool to determine the creep closure of the cavern over long time periods. The ABAQUS Explicit solver package® was used to develop the finite element model of the cavern, and to study the creep behavior of the cavern and the developed stresses under the overburden and gas pressure inside the cavern. The creep model developed in the experimental studies was assigned to the salt material to study a 5-year creep behavior. Different scenarios for the cavern aspect ratio and the gas pressure inside the cavern were assumed, and the developed state of stress (effective, normal, tangential, and shear stress) were calculated. Also, the displacement values and contours were determined for each analysis, which clearly depicted the closure direction and severity. The state-of-the art numerical modeling of the cavern can be found in the literature review section.

A criterion is required to evaluate the results of the numerical or experimental analyses of the caverns under any state of stress. The creep in the salt causes an irreversible dilatancy, and, therefore, the stress-based dilatancy criteria were considered in most of the failure theories in salt caverns under any state of stress (e.g. [2-6]). This envelope is based on the first invariant of the effective stress tensor (I_1) and the second invariant of the deviator stress tensor (J_2). Based on the Mohr-Coulomb failure envelope and the friction angle of the salt, a dilatancy failure envelope was developed in this study to evaluate the state of stress and damage of the cavern under scrutiny.

The numerical model developed in this study is a tool for developing the key engineering design guidelines regarding the underground salt caverns in the Fischells Brook area in western Newfoundland. Section 2 introduces the site location and surface description, and reviews the relevant literature about the deformation behavior of the salt rock, creep models, failure criteria, and numerical studies of the underground salt caverns. Section 3 describes the experimental setup and the tests performed to develop a creep model of the salt rock. Sections 4 and 5 present a review of the developed numerical model and design scenarios of the cavern geometry and operating pressures and numerical simulation results, and a discussion of the design parameters. Section 6 is comprised of a discussion, conclusions, and future research directions.

2. Literature review

2.1. Rheology and time-dependent deformation behavior of salt rock

Low permeability and high ductility are the factors that make a salt rock an ideal material for underground gas storage. A homogenous rock salt

mainly consists of halite with a grain size of 1-50 mm, and the internal friction angle ranges from 35° to 40° [7]. In the elastic deformation region, the salt rock is molded using the Hook's law. In the inelastic region, the actual deformation behavior of the salt is dominated by the time-dependent deformation (creep). The creep behavior of the salt rock can be divided into three major stages: transient, steady-state, and tertiary. In the first stage of the creep, the creep rate is decelerating, and the creep deformation may be recovered. In this stage, the creep rate decreases until it reaches a steady-state rate. In the second stage, the creep rate is constant, and the creep deformation is not recoverable. In this stage, the creep continues indefinitely under constant loading. In the last stage (tertiary creep), the creep rate is accelerating toward rupture. The tertiary stage is not of engineering interest in salt rock, as it happens at high strain rates in the laboratory, not in situ conditions with much lower strain rates [1]. In the engineering range of stress and temperatures, the rock salt undergoes both the transient and steady-state creep, and it is the geological time interval which dictates the creep regime of the material. At slow strain rates (less than 10^{-6} s^{-1}), the salt can continue to deform indefinitely in the steady-state stage without undergoing internal damage leading to tertiary creep. The creep is more rapid in conditions with higher temperatures, higher differential stress, and higher depth. This means that the closure of the cavern is always an engineering consideration while developing salt caverns.

Rheological models of salt creep range from elastic creep models with and without creep recovery to viscoplastic models [8, 9]. Generalized visco-elasticity models with creep recovery are a proper engineering approximation for creep models of salt caverns. The viscoelastic and visco-plastic models have been studied by many researchers in the last 30 years [10, 11]. Moreover, experimental studies have been conducted to validate the developed models. The most widely used steady-state creep salt model is the Norton creep law (also called the power-law creep model), which is based upon the steady-state strain rate and the maximum deviatoric stress difference [12, 13]:

$$\dot{\epsilon} = A(\sigma_1 - \sigma_3)^n \exp(\frac{-Q}{RT}) \quad (1)$$

where $\dot{\epsilon}$ is the steady-state strain rate, A is an empirically-measured material-dependent parameter, σ_1 and σ_3 are the principal stress values, T is the temperature in kelvin, R is the universal gas constant, and Q is the activation energy of the given mechanism. The exponent n is the stress component, which should be evaluated empirically for different salt rocks. The exponent n in the power law equation can be determined by conducting a series of experiments at different stress levels at a constant temperature. Frayne et al. [14] have analyzed three mines (700-1050 m of depth) and long-term public domain creep data, and have concluded that n = 3 works in several practical mines and caverns [14, 15].

The power law equation in a constant temperature test can be simplified as [12]:

$$\dot{\epsilon} = A^*(\sigma_1 - \sigma_3)^n \quad (2)$$

The creep models for the commercial finite element packages can be categorized as the time-hardening creep law, strain-hardening creep law, and Singh-Mitchell creep law.

The first model, which is a form of the power law creep model, is the most common one used, while the stress in the material remains essentially constant:

$$\dot{\epsilon} = A^*(\sigma_1 - \sigma_3)^n \quad (3)$$

The A and n values are the inputs to the FEM models, and can be determined using the experimental creep studies.

2.2. Failure criteria for creep-induced damage of salt rocks

As mentioned earlier, the salt under the shear stress developed by the in situ stress and cavern pressure creeps (dilates), resulting in micro-fracturing and weakening of the cavern roof. In other words, the shear stress as a result of the creep goes above the shear strength of the salt. A criterion is required to interpret the results of the numerical or experimental analyses of the gas caverns under any state of stress. Chan et al. [16] have investigated three creep rupture criteria, the dilatancy, minimum strain rate, and damage variable criteria. The creep in salt causes irreversible dilatancy and, therefore, the stress-based dilatancy criteria have been considered in most of the stability analyses of the salt caverns (e.g. [2-6]).

All the developed salt dilation criteria are based on the envelope developed by the experimental creep analyses for the first invariant of the effective stress tensor (the value for the excess pore fluid pressure is subtracted from that for the stress tensor) and the second invariant of the deviator stress tensor. Spiers et al. [17] have conducted a constant strain rate in triaxial

compression stress experiments, and have derived a linear relationship between the first invariant of the stress tensor and the second invariant of the deviator stress tensor in units of MPa:

$$\sqrt{J_2} = 0.27\, I_1 + 6.4 \quad (4)$$

In another study, Ratigan et al. [18] have developed a criterion based on the volumetric strain rate as negative for the non-dilating boundary and positive for the dilating boundary. The dilating and non-dilating boundaries were presented as a linear relationship between the first invariant of the stress tensor and the second invariant of the deviator stress tensor in units of MPa:

$$\sqrt{J_2} = 0.27\, I_1 \quad (5)$$

Also, Hunsche [19] has conducted triaxial tests to measure the volumetric strain values, and acoustic emission rate to develop a dilatancy/compressibility envelope. The volume increase is called dilatancy, and the volume decrease is called compressibility. The dilatancy envelope developed by Hunsche [19] is in terms of the octahedral shear stress and octahedral mean stress, and can be converted to an envelope in terms of the first invariant of the stress tensor and the second invariant of the deviator stress tensor:

$$\sqrt{J_2} = \sqrt{1.5}\left(f_1 \frac{I_1^2}{9} + f_2 \frac{I_1}{3}\right) \quad (6)$$

Mean stress [20], intermediate stress [21], temperature [6], pore pressure [22, 23], and bedding plane orientation are the variables that affect the dilatancy envelope of salt. The previously discussed dilatancy envelopes did not consider the mean stress (the envelope had no intercept on the $I_1 - \sqrt{J_2}$ plot). Moreover, the developed envelopes were linear, and did not consider the Lode angle effect. A new method for developing a stress-based dilation envelope considering the above fact has been proposed by DeVries et al. [20], and the goal was to enable the comparison of the stress state determined around a cavern by the experimental tests. DeVries et al. [20] have implemented a power fit on the data points of the values for the second invariant of the deviator stress tensor and the first invariant of the stress tensor. This theory is based on the projection of the stress components to the π-plane (the vertical plane to the hydrostatic axis). Due to this projection, the neglected effect of the Lode angle and the mean stress in the older criteria are considered. In this model, the Mohr-Coulomb failure theory in triaxial extension-compression is rearranged in terms of stress invariants:

$$\sqrt{J_2} = \frac{S_0 \cos\varphi - \sigma_m \sin\varphi}{\frac{\sqrt{3}}{2}\left(1 \pm \frac{\sin\varphi}{3}\right)} \quad (7)$$

Where the $+$ sign is for extension and the $-$ sign is for compression. S_0 is the material cohesion, φ is the internal friction angle, σ_m is equal to $I_1/3$ (one third of the first stress invariant), and J_2 is the second invarient of the deviator stress tensor. In the most conservative case, where the internal friction angle is considered as zero, the equation can be simplified to:

$$\sqrt{J_2} = \frac{2S_0}{\sqrt{3}} \quad (8)$$

The above equation could be considered as a power law fit in the $I_1 - \sqrt{J_2}$ plot. The values for $\sqrt{J_2}$ and I_1 for different types of salts can be determined using the triaxial test or uniaxial test accompanied by the Mohr failure envelope for a certain friction angle. The method proposed by DeVries et al. [20] was implemented in this study to develop a dilatancy failure envelope for the salt rocks drilled in the Fischells Brook area.

2.3. Numerical studies of underground salt caverns

During the last 10 years, various studies have been performed to study the cavern stability and investigate the parameters affecting it. In all of these models, an empirical creep model has been developed and imported to the numerical model. The overburden was modeled with either the elastic models or the classic Mohr-Coulomb model. The finite element or finite difference computational schemes were implemented to integrate the models, and parametric studies were performed to study the effects of the cavern roof thickness, operating pressure, geometry and overburden stiffness on the stability and closure of the cavern.

Hoffman and Ehgartner [24] have developed a 3D finite element model to investigate the effects of a number of caverns on storage losses, surface subsidence, and cavern integrity. Using an accumulated stability criterion, the larger cavern fields are expected to have a shorter life. Adams [25] has developed guidelines for the gas pressure inside the cavern using a 2D finite element model. The minimum and maximum gas pressure and the proper distance between the adjacent caverns were investigated. DeVaries et al. [20] have developed

a finite element model to evaluate the effects of the cavern design parameters (roof thickness, depth, and aspect ratio) on the minimum allowable gas pressure of the cavern. They developed a new dilatancy criterion to evaluate the simulation results. The results obtained have shown that the state of stress is alternating between tension and compression near the wall of the cavern. Han et al. [26] have developed a finite difference model in FLAC3D® for a single-bedded salt cavern. A viscoplastic Drucker-Prager represented the salt formation and an elastic or Mohr-Coulomb model for the non-salt formations. They studied the cavern damage over a year and a 15-year time period. Moreover, parametric studies were performed to study the effects of roof thickness, overburden stiffness, and cavern geometries on its stability. It was concluded that deformation is high around the cavern roof and corners, while the stress is high around the cavern wall and hydrostatic pressure results under the most stable cavern conditions. Also, large caverns were found to be less stable compared to the small ones, while a thick cavern roof increases the stability of the cavern, and a softer overburden results in the spall of the cavern roof. Ardeshiri and Yazdani [27] have studied the influence of faults on the seismic behavior of the underground caverns using the FLAC2D® explicit finite difference program. A dynamic non-linear analysis was performed under an earthquake ground motion at the bottom of the model. It was concluded that the most critical state of the damage is the case when the fault intersects the cavern roof. Hilbert and Exponent [28] have investigated the casing failures associated with the caverns in bedded salt domes using a finite element model. It was concluded that a low-gas pressure in the cavern causes damaging tensile stress in the casing, while a high-gas pressure results in the micro-fracture of the cavern and instability of the cavern roof. They also concluded that the location of the casing shoe and the input gas temperature are important in the casing failure. Ma et al. [29] have investigated the convergence of salt caverns in an ultra-deep formation at high temperatures using the creep tests. They conducted experiments to investigate the effect of temperature and deviatoric stress on the creep behavior of the salt samples drilled in the Jianghan basin. It was found that the effect of the deviatoric stress was greater than the effect of temperature on the creep behavior. Then, using the creep model developed in the experiments, they developed a finite element model for a cavern with a certain volume, and imported the model to FLAC3D® for a geo-mechanical analysis to study the effect of the cavern pressure on its convergence ratio and volume loss. It was concluded that the injection and withdrawal of the gas did not affect the convergence ratio, whereas the inner pressure affected the convergence by a linear relationship. Nazary Moghaddam et al. [30] have developed a Lagrangian finite element formulation of the salt cavern with an elasto-viscoplastic constitutive model for the salt to evaluate the dilatancy and creep of the cavern in short terms (SFR) and long terms (LFR). Peric's viscoplastic model has been implemented to model the transient creep, and the Cristescu's steady-state model has been used to study the stead-state creep. The stress variation and ground movement were investigated for an axisymmetric model of the cavern. A detailed explanation of the finite element model developed in this research work can be found in section 4.

3. Experimental investigation

3.1. Site location and surface description

The Fischells Brook area is located in the St. George's Bay area of southwest Newfoundland, 10 km south of the St. George's basin, flowing east to west. The rocks at St. George's Bay are from part of a carboniferous basin extending from New Brunswick and Nova Scotia to southwest Newfoundland, filled predominantly with non-marine clastic sediments but with an incursion of deposits in a long narrow basin trending NE, overlying a basement of older rocks. Fischells Brook is a pillow-shaped body of salts that ascends 800-900 m from its stratigraphic level and invades the overlying rocks, rather than having a classical dome. It was discovered in the 1950-1960's during a gravimetric survey of the St George's carboniferous basin, which was known to contain evaporite horizons and anhydrite mined at several places. The location of the Fischells Brook area is depicted in Figure 1.

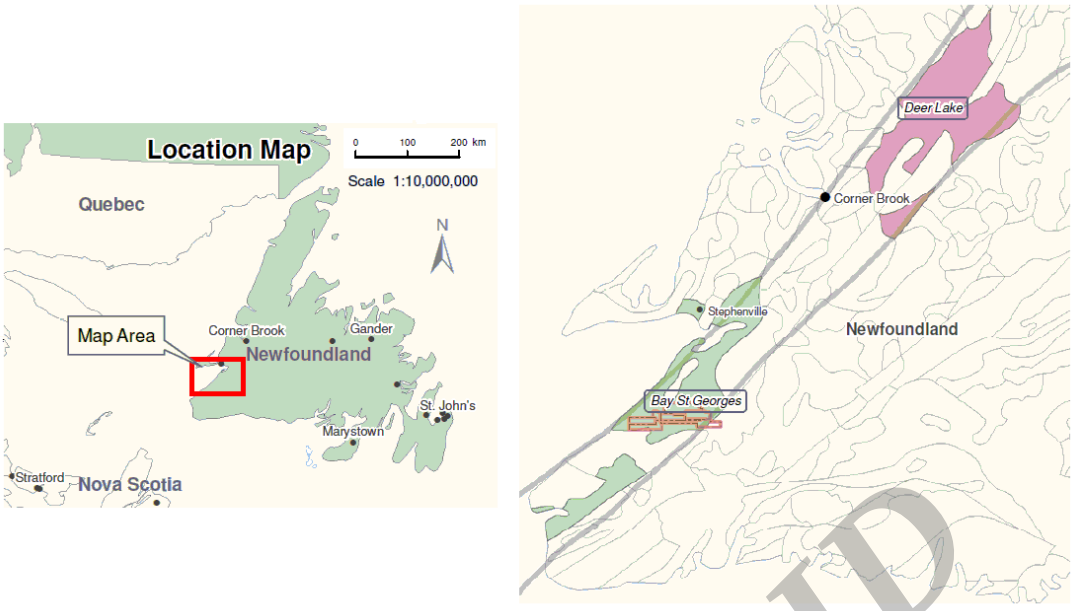

Figure 1. Fischells Brook area in southwest Newfoundland [31].

Fischells Brook consists of 3 salt units, the upper and middle halites, which include many clay beds, some K-salts and minor anhydrite and the basal halite, comprising a great thickness of massive rock salt. The rocks at St George's Bay are filled mainly with non-marine clastic sediments, in which a sequence of evaporites and limestones are precipitated. The gray shale layer is the top layer, which has insoluble residues left from the salt dissolution. Fischells Brook is a typical diapir of salt that rose 700-800 m from its original level, and is pillow-shaped with gently-sloping sides and ends rather than a steep-sided dome. The minerals available in the formations are Halite, Sylvite, Carnallite, Polyhalite, Anhydrite, and Gypsum.

3.2- Multi-stage creep test

Creep tests are usually conducted to develop a constitutive law for engineering materials. Three types of tests are common in the engineering creep studies: constant stress tests, constant strain rate tests, and relaxation tests, for which a strain increment is applied. Among these three tests, the constant stress test is ideal for deterring the steady-state creep behavior of the salt, which is useful for the numerical modeling of the salt rock cavern over a long period [1, 32]. Servo hydraulic compression test machines have been widely used to maintain the constant load during the creep test. However, the servo hydraulic machines are not financially efficient for long creep tests. In this investigation, a hydraulic frame actuator is selected to achieve the target stress level. Multi-staged constant stress tests are performed for this investigation based on the stress levels that are representative for the depths of the Fischells Brook deposit. The stress levels are 7.5, 10, and 15 MPa. A hydraulic valve is located between the hydraulic jack and hydraulic cylinder to maintain the stress level in the target stress once the pressure is applied. The creep tests were performed based on "ASTM D7070" [32]. A scheme of the creep test rig developed for this investigation is shown in Figure 2.

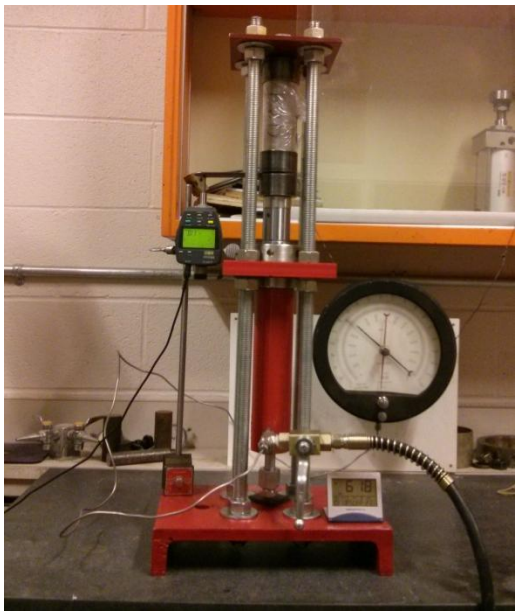

Figure 2. Scheme for creep test rig.

The core specimens in this study are retrieved from the NLDNR Core Storage Facility in Pasadena, Newfoundland for the geo-mechanics characterization. Three units within the Fischells Brook salt deposit (upper, middle, and basal halite) are under study. Visually, the upper halite

appeared to have some components of reddish crystals, possibly potash, while the other 2 units appeared to be predominantly halite. These specimens were prepared as "ASTM D4543-08" [33] to the right circular cylinders with a length to diameter ratio of approximately 2.0 to 2.1. The samples were cut by a hand saw without any water and ground flat and square using a grinding jig. The end flatness and parallelism tolerances are checked with procedure PF2. The moisture condition qualitatively is "as-received", and the samples are kept in plastic bags to keep the moisture as constant as possible during the tests. A dial gauge is mounted on a rigid base to measure the axial displacement of the sample. The data points are recorded for each test in reasonable time intervals. A line is fitted to the steady-state level of each test. The stress level in each step is increased after reaching the steady-state strain rate. Two samples in each group were tested. The creep behavior of one of the upper halite samples is shown in Figure 3, and the associated creep rate in 15 MPa is shown in Figure 4.

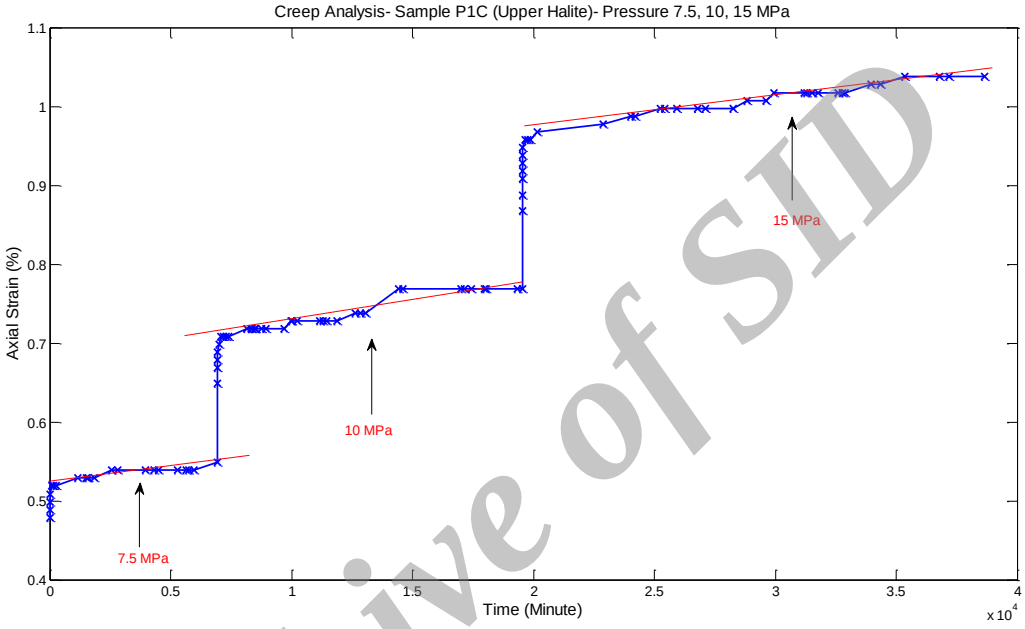

Figure 3. Multi-stage creep test of upper halite sample.

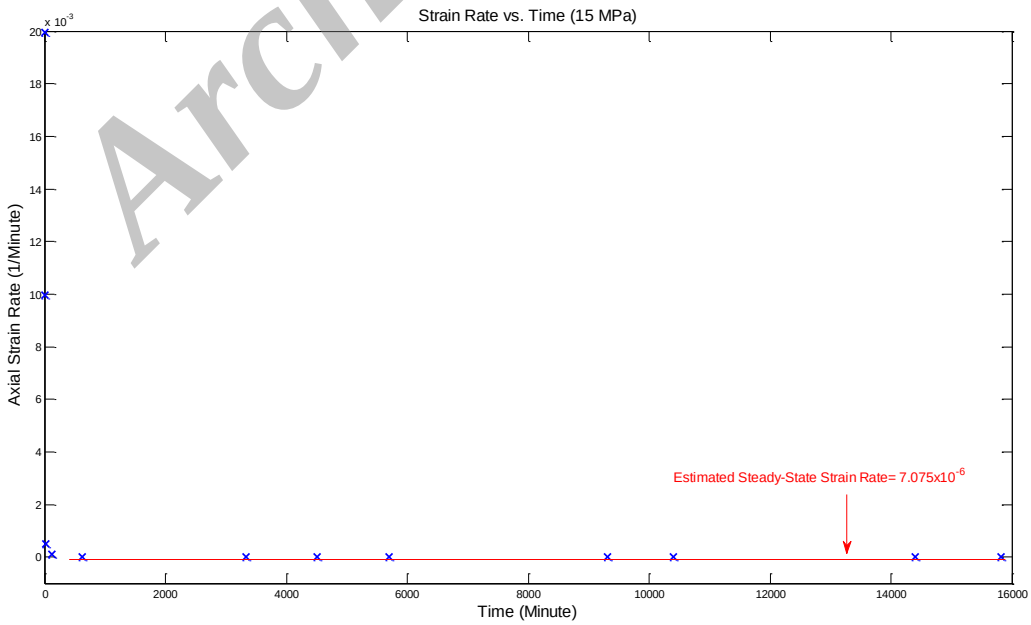

Figure 4. Estimated strain rate for upper halite sample in 15 MPa.

The results of the axial strain for one of the middle halite samples and for one of the basal halite samples are shown in Figures 5 and 6. The same procedure was implemented to determine the strain rate for the middle halite and basal halite samples, and the estimated strain rates for the samples are summarized in Table 1.

Based on the estimated strain rates of three types of salt rocks and the applied stress in uniaxial tests, the A^* and n values are calibrated for implementation in the developed FEM models, as follow in Table 2.

Since the state of stress is important in the overburden formations, the UC tests of the overlying formations (sandstone and shale) and the Mohr-Coulomb failure envelope were also developed in this study. Based on the UCS test results, the average UCS value for the sandstone is estimated to be 13.73 MPa, and the average UCS value for the shale is 43.14 MPa. For each type of Sandstone and Shale, two specimens are tested.

Since the dilatancy envelope requires the hydrostatic difference to determine the deviatoric stress tensor, uniaxial tests for the basal halite cores are performed to develop a Mohr-Coulomb failure envelope. In this investigation, two uniaxial tests are conducted, and an average UCS value of 35 MPa is recorded (Figure 7).

It has been shown that most of the salt rocks have a friction angle between 35^{o} and 40^{o} [34]. Based on an average value for the friction angle (37.5°), the uniaxial test results could be implemented to develop the Mohr failure envelope. Using the average UCS test of basal halite and the average friction angle, the Mohr envelope of basal halite is developed, and sketched in Figure 8.

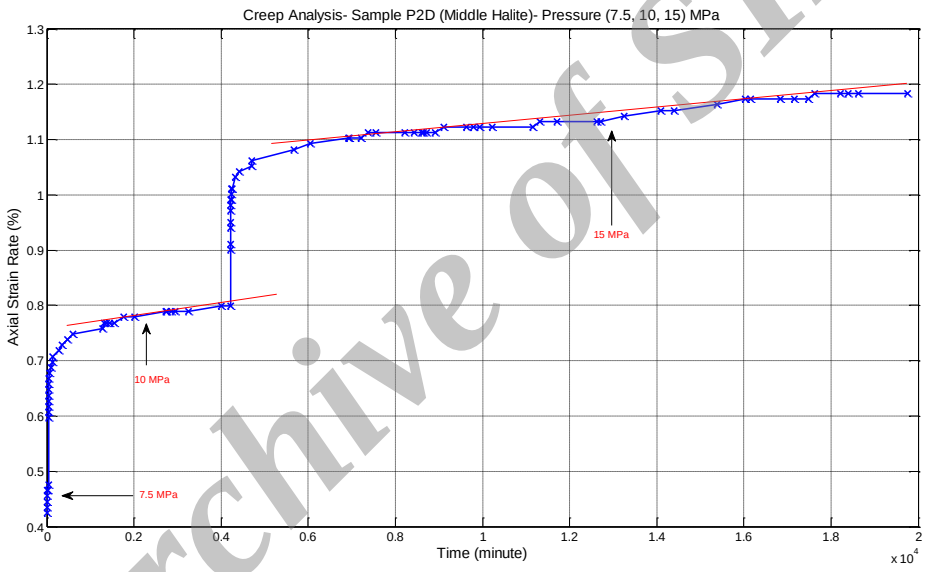

Figure 5. Multi-stage creep test of middle halite sample.

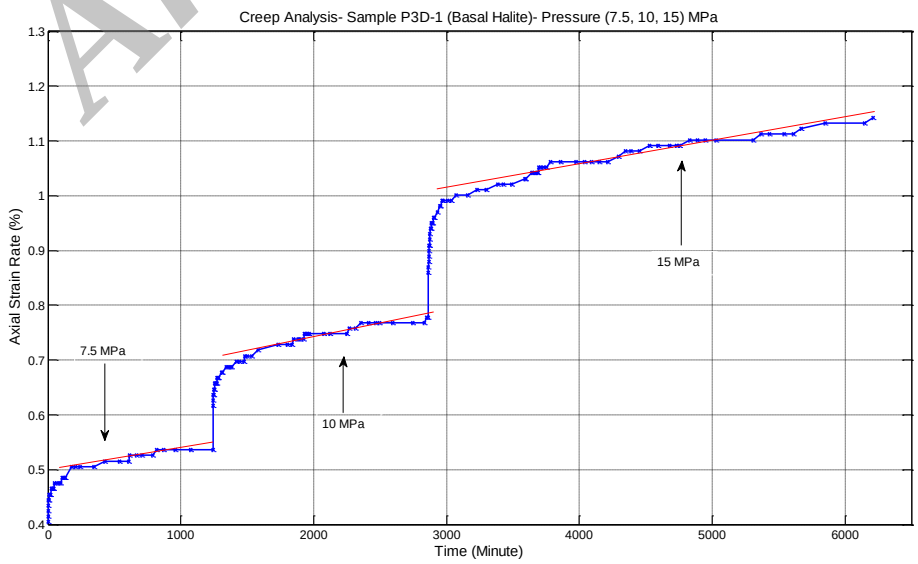

Figure 6. Multi-stage creep test of basal halite sample.

Table 1. Estimated steady-state strain rate for three types of salt rocks.

Stress level (MPa)	Upper halite content (1/min)	Middle halite (1/min)	Basal halite (1/min)
7.5	2.28×10^{-6}	4×10^{-7}	5.32×10^{-7}
10	2.20×10^{-6}	1.048×10^{-6}	5.043×10^{-7}
15	7.075×10^{-6}	1.56×10^{-7}	8×10^{-7}

Table 2. Power law creep multiplier and exponent values for different salt rocks

Salt type	A^*	n
Upper halite	2.096×10^{-27}	3
Middle halite	4.622×10^{-29}	3
Basal halite	2.37×10^{-28}	3

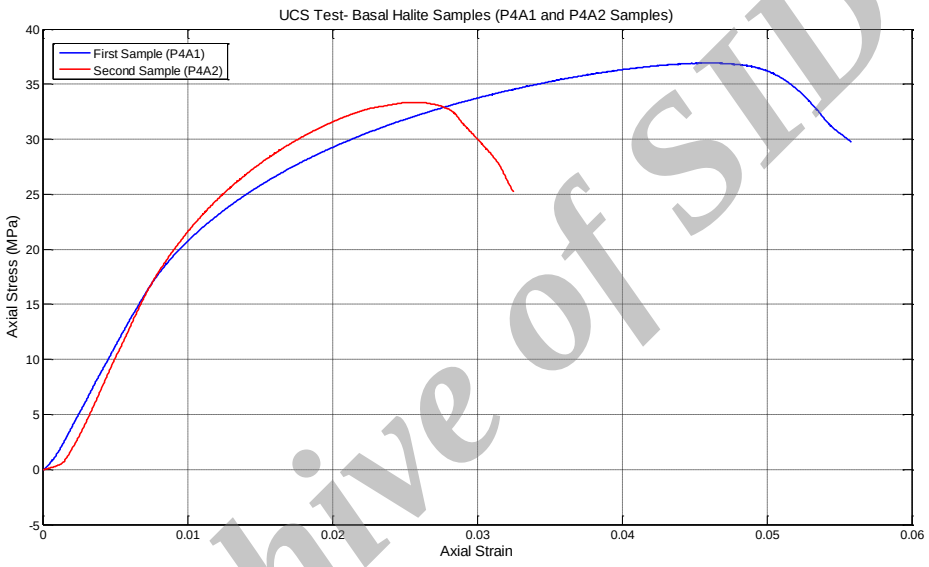

Figure 7. UCS tests for basal halite.

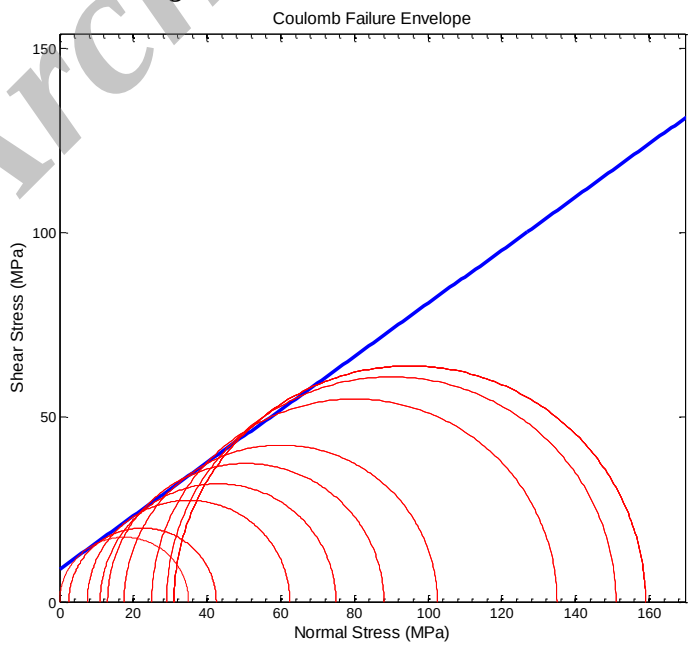

Figure 8. Mohr failure envelope for basal halite.

The values of $\sqrt{J_2}$ and I_1 can be determined using a triaxial test or uniaxial test accompanied by the Mohr failure envelope for a certain friction angle. In a triaxial test, the stress tensor is written as:

$$\sigma = \begin{bmatrix} \sigma_{11} & \tau_{12} & \tau_{13} \\ \tau_{21} & \sigma_{22} & \tau_{23} \\ \tau_{31} & \tau_{32} & \sigma_{33} \end{bmatrix} = \begin{bmatrix} \sigma_1 & 0 & 0 \\ 0 & \sigma_3 & 0 \\ 0 & 0 & \sigma_3 \end{bmatrix} \quad (9)$$

where σ_1 is the overburden pressure, and σ_3 is the confining pressure. The invariants of the stress tensor and the deviator stress tensor are determined as:

$$I_1 = \sigma_{11} + \sigma_{22} + \sigma_{33} = \sigma_1 + 2\sigma_3 \quad (10a)$$

$$I_2 = \sigma_{11}\sigma_{22} + \sigma_{22}\sigma_{33} + \sigma_{11}\sigma_{33} - {\sigma_{12}}^2 - {\sigma_{23}}^2 - {\sigma_{13}}^2 = 2\sigma_1\sigma_3 + {\sigma_3}^2 \quad (10b)$$

$$J_2 = \frac{1}{3}{I_1}^2 - I_2 = \frac{1}{3}(\sigma_1 + 2\sigma_3)^2 - (2\sigma_1\sigma_3 + {\sigma_3}^2) = \frac{1}{3}(\sigma_1 - \sigma_3)^2 \quad (10c)$$

Different values of σ_1 and σ_3 were recorded using the Mohr envelope, developed in Figure 8. Then, the corresponding I_1 and J_2 values were determined using the above equations, and plotted as data points on the $\sqrt{J_2}$ -I_1 plot. Then, a power fir model is implemented to develop the dilatancy failure envelop, as depicted in Figure 9. This envelope will be used to evaluate the numerical results of the FEM model in this study.

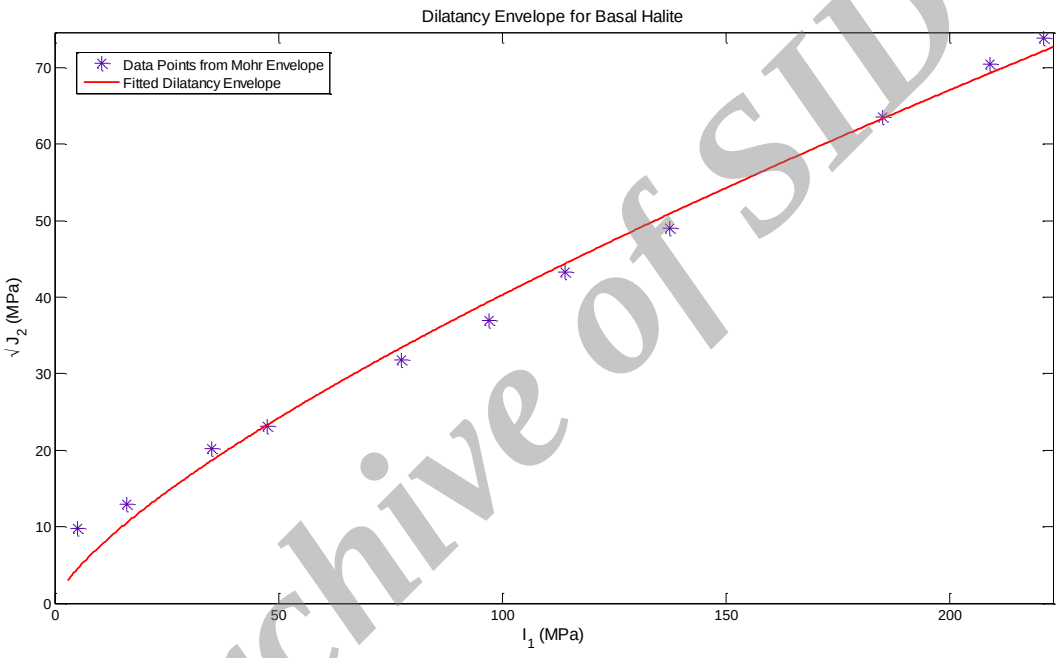

Figure 9. Dilatancy failure envelope for basal halite.

4. Finite element modeling of underground caverns

The ABAQUS Explicit solver package® is used to develop the finite element model of the cavern, study the creep behavior of the cavern, and develop the stresses under the gas pressure stored inside the cavern. Natural gas caverns are usually created by the dissolution process, and the normal shape of the developed cavern is oval. Based on the map of the salt rock deposits in the Fischells Brook area, the cavern is located inside the homogenous basal halite. The overlying formations are 100 m of sandstone, 100 m of shale, and 200 m of upper and middle halite. The depth of the basal halite is 900 m. Four different scenarios are considered for the geometry of the cavern based on the aspect ratio (L/d) of the cavern. The caverns are considered to have the diameters 100, 200, 300, and 400 m, while the length of the cavern is considered as 400 m. A scheme for the cavern and the overlying formations are shown in Figure 10.

An axisymmetric model is considered for the numerical analysis, as shown in Figure 11.

Four different material types are defined for the formations present in the model, and each material is assigned to a specific formation. In order to use the "SOIL" analysis in ABAQUS® for creep studies, the permeability of the pore fluid should be defined through the hydraulic conductivity and void ratio. The creep behavior is assigned to each material based on the coefficients defined in Table 2. The material properties defined in the FEM model are summarized in Table 3.

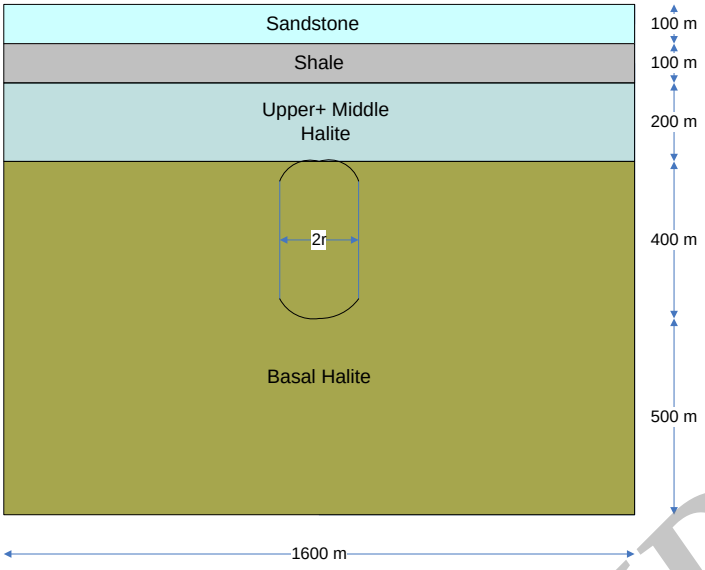

Figure 10. Scheme for formations and cavern model in Fischells Brook area.

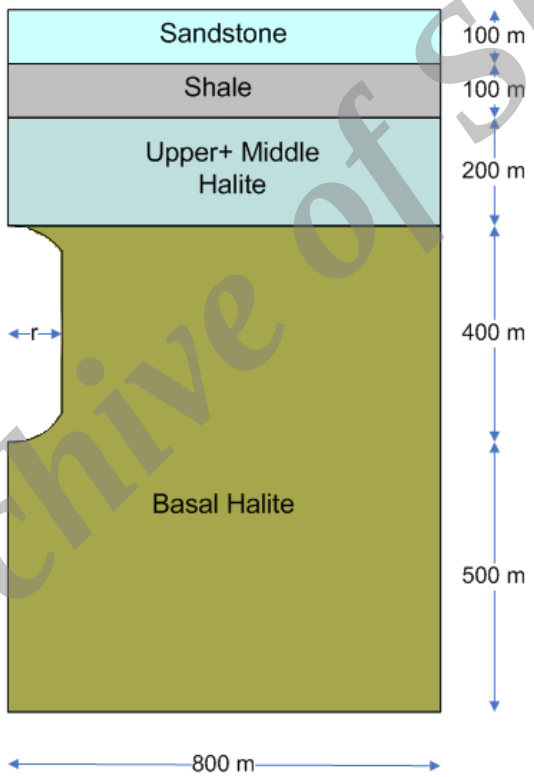

Figure 11. Axisymmetric model for cavern and formations.

Table 3. Material properties of different formations in FEM model.

Material	Density (kg/m^3)	Young's modulus (GPa)	Hydraulic conductivity	Poisson's ratio
Sandstone	2500	30	NA	0.4
Shale	2500	30	NA	0.4
Upper and middle halite	2200	30	1×10^{-12}	0.4
Basal halite	2200	30	1×10^{-12}	0.4

The gas pressure inside the cavern is assumed to be 6 MPa. The axis of symmetry is defined on the left side of the model and the right and bottom sides of the model are bounded by the roller-type boundary conditions. Gravity is applied to the entire model.

A "GEOSTATIC" analysis is defined as the first step analysis, which applies gravity to the model to equilibrate geostatic loading of the finite element model. The second step is the "SOIL" analysis to equilibrate any creep effects induced from the initial geostatic loading step. The non-linear effect of the large deformations is also considered in the creep analysis. The initial time step is defined as 10^{-7} s, and an automatic time incrimination with a maximum increment of 100 s is selected. The creep is modeled in a 5-year period.

An element size of 100 m is selected for the analysis, and a mesh convergence analysis is conducted to ensure the accuracy of the results with the selected size of the element. The "CAX8RP" elements are assigned to the entire model, which is an appropriate element in the presence of the pore pressure. This is an 8-node axisymmetric quadrilateral, biquadratic displacement, bilinear pore pressure, reduced integration element. Reduced integration is recommended when second-order elements are used to achieve more accurate results and less computational time. The models of different scenarios are developed, and the FEM analyses are conducted for all assumed scenarios. The stress and displacement values are recorded in 10-minute increments.

5. Simulation results and discussion

The cavern diameter varies from 100 to 400 m, with an increment of 100 m. The massive salt rock in Fischells Brook starts at a 400 m depth from the surface, and continues up to 1300 m from the surface, and the cavern length of 400 m starting at a 400 m depth is considered in this study.

The in situ pressure distribution at the end of the "GEOSTATIC" step is shown in Figure 12, which is equal to the weight of the overburden. This pressure gradient will be propagated to the next step of the analysis, and is considered as an initial condition for inducing the creep behavior.

The radial displacement for all the four scenarios after 5 years of creep is shown in Figure 13. The radial displacement varies from 29 cm for a cavern with a diameter of 100 m to 55 cm for a cavern with a diameter of 400 m.

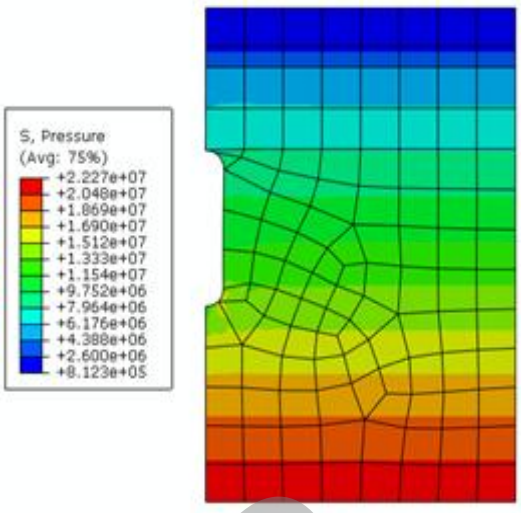

Figure 12. Pressure distribution after GEOSTATIC step.

The radial displacement along the center line of the cavern is compared for the four scenarios in Figure 14, which verifies that the displacement is the highest for a cavern with the largest diameter.

The resultant vertical displacement and the radial displacement for the four scenarios are shown in Figure 15, which shows the direction of the closure of the cavern after 5 years. The closure increases with increase in the cavern diameter.

The state of stress around the cavern is related to the overburden formation, cavern depth, and cavern pressure. The stress distribution for the caverns with the diameters 100, 200, 300, and 400 m are shown in Figures 16-19, respectively.

It is obvious that with increase in the cavern diameter, the affected shear stress area extends to a further distance with a higher value near the corner of the cavern. The developed shear stress is the main reason for the salt dilatancy near the cavern, and with increase in the cavern diameter, the possibility of dilatancy is expected to increase. This fact can be verified by plotting the corresponding state of stress in the plot of the dilatancy failure envelope. In order to depict the state of stress in the dilatancy failure envelope, the maximum principal stress values are determined in each scenario, and, based on Eq. 10, the values of I_1 and J_2 are determined. The corresponding states of stress for the caverns with the diameters 100 to 400 m are shown in Figure 20. As it was expected, with increase in the cavern diameter, the dilatancy of the surrounding salt increased, and the state of stress approached the failure state in the dilatancy plot.

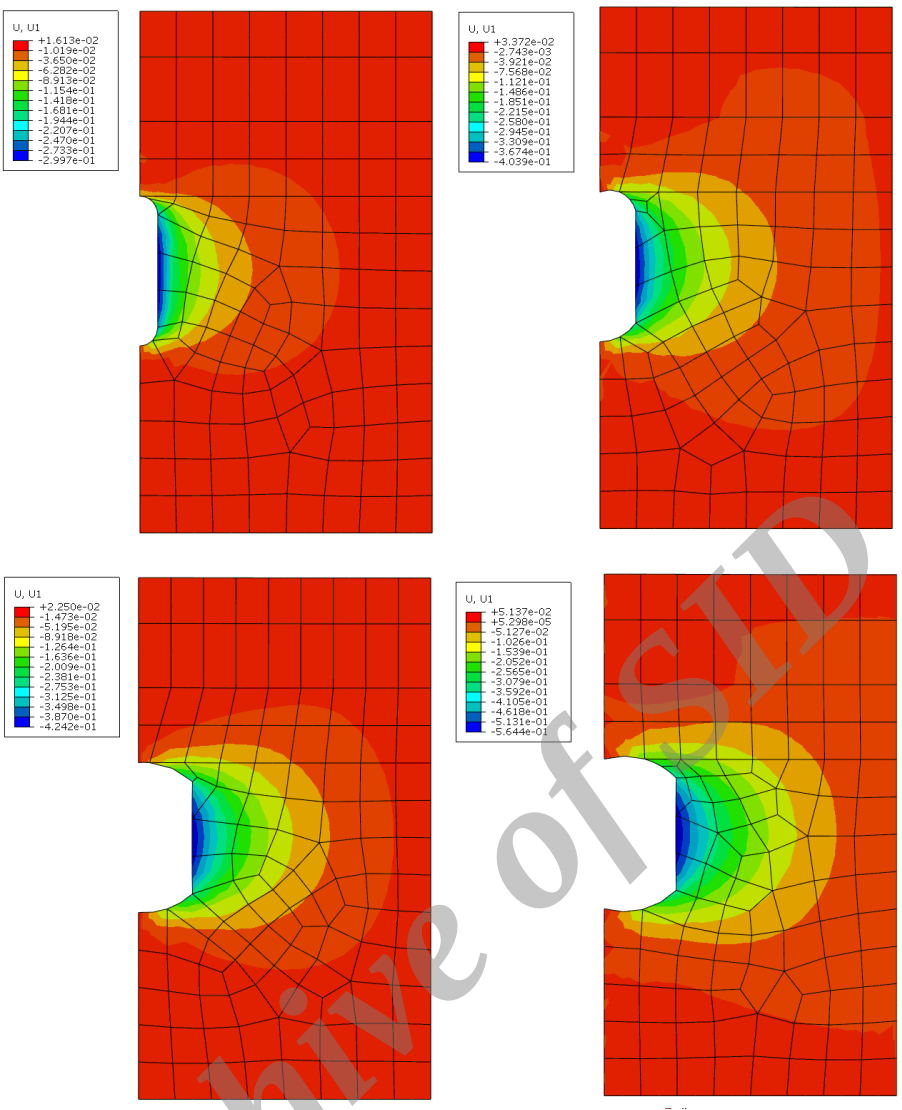

Figure 13. Radial displacement for four scenarios of cavern diameter after 5 years of creep.

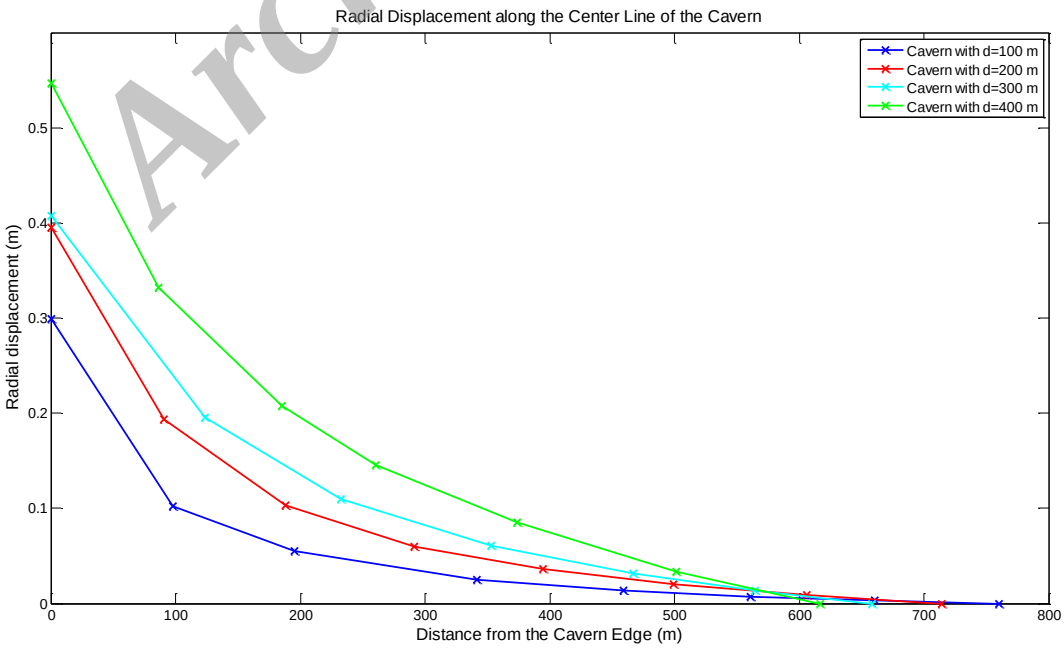

Figure 14. Radial displacement along center line of cavern after 5 years.

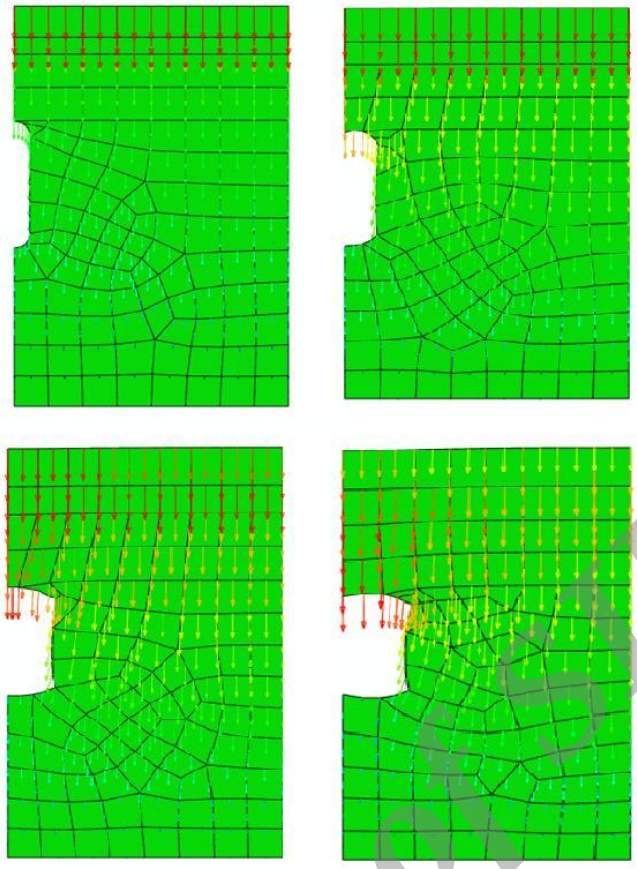

Figure 15. Resultant deformation of cavern after 5 years.

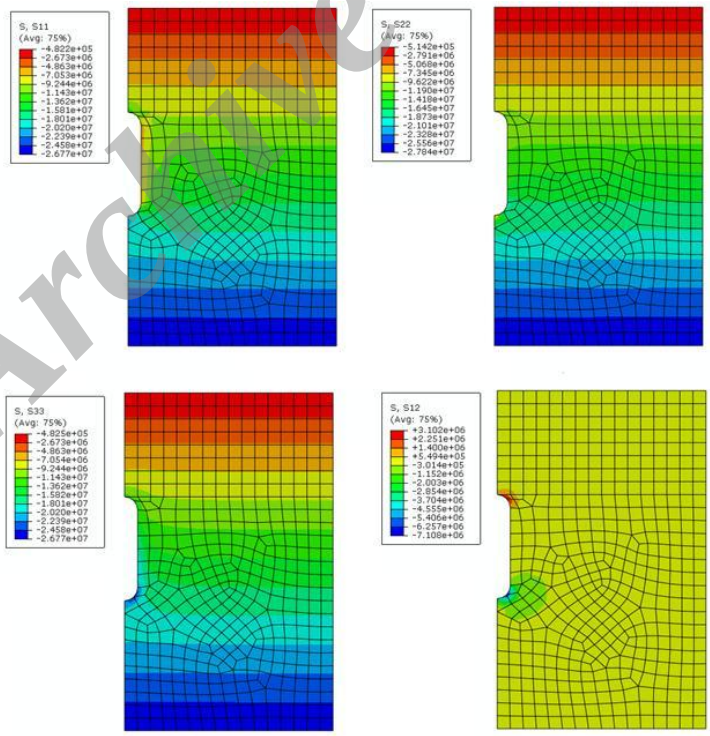

Figure 16. Radial, vertical, tangential, and shear stresses for cavern with d=100m.

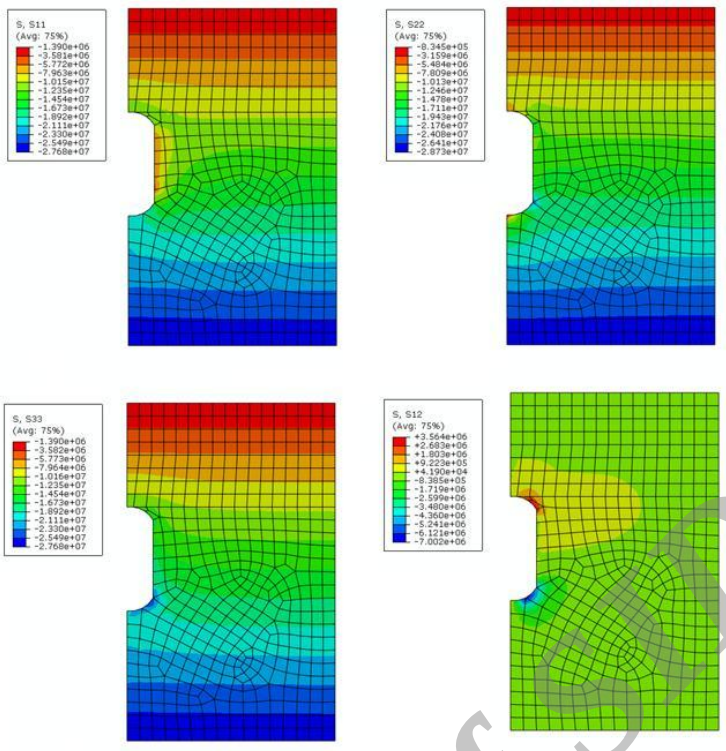

Figure 17. Radial, vertical, tangential, and shear stresses for cavern with d=200m.

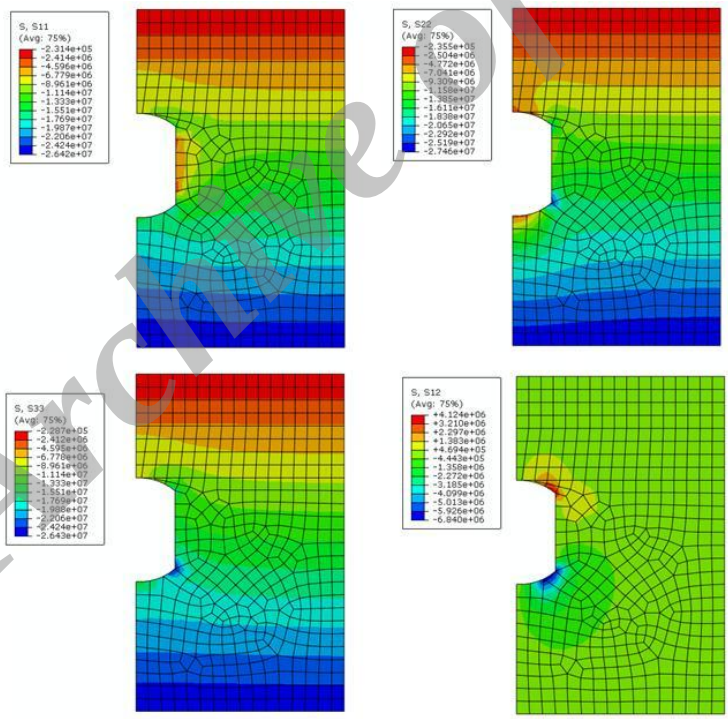

Figure 18. Radial, vertical, tangential, and shear stresses for cavern with d=300m.

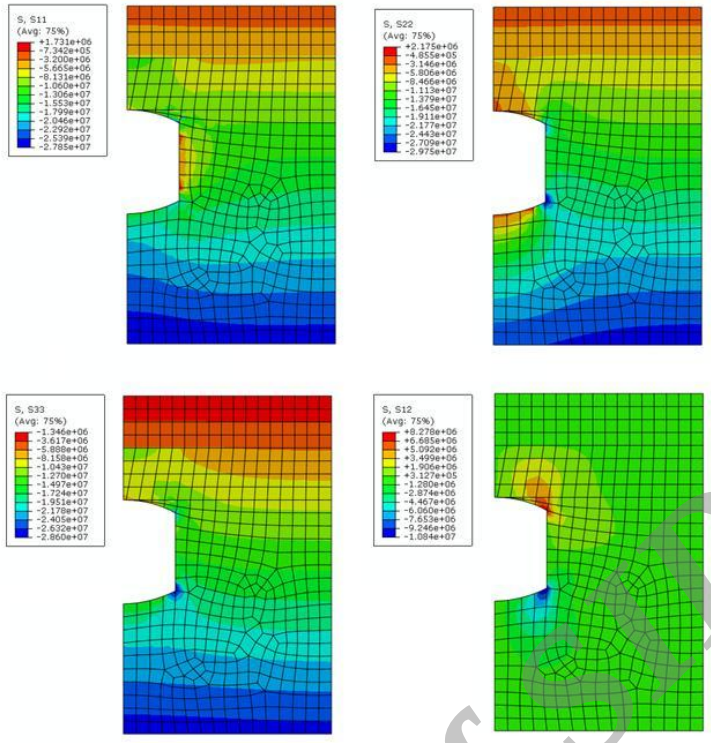

Figure 19. Radial, vertical, tangential, and shear stresses for cavern with d=400m.

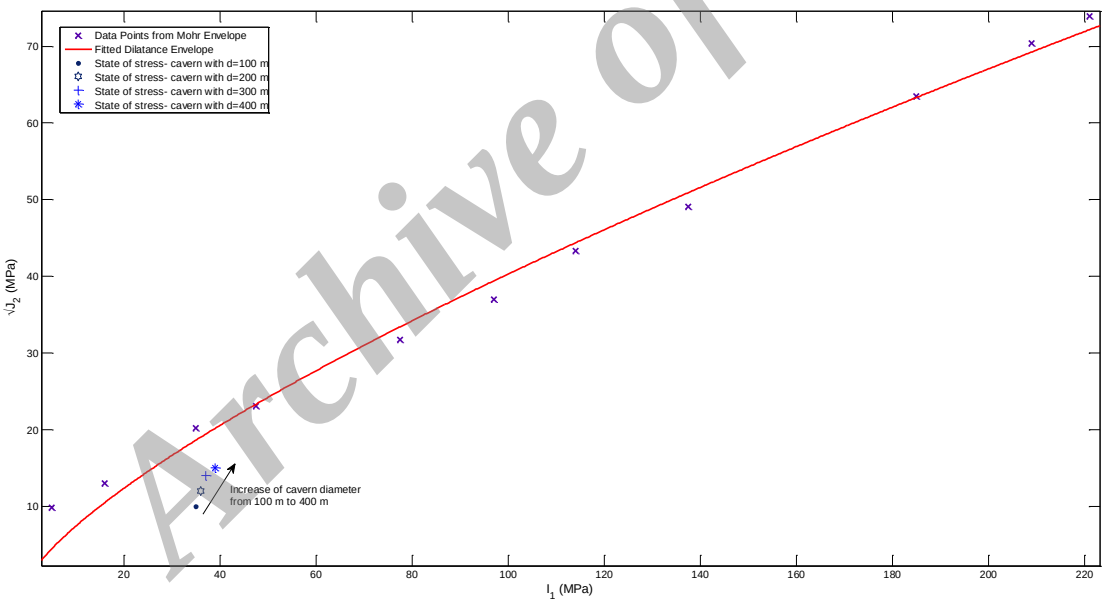

Figure 20. Corresponding state of stress for caverns with diameters of 100, 200, 300, and 400 m.

Equivalent Von Mises stress is a factor that shows the zones of high shear stress, and is a proper parameter to determine the spacing with the neighboring cavern and pillar sizing. The affected stress area is shown as a contour-plot in Figure 21, which depicts that the stress affects an area close to the cavern. It is clear that with increase in the cavern diameter, the affected stress area extends to a further distance. Moreover, the horizontal stress rapidly increases at the cavern wall, and it is the same as the vertical stresses far away from the cavern wall. The stress-affected area is about 2.5 times the diameter of the cavern, and, after this distance, the vertical and horizontal components were the same. In other words, the stress components drop off to the in-situ stress within a distance equal to a five-cavern radius. Based on the stress-affected area results, the distance of a five-cavern radius is suggested for the pillar width. The finding for the pillar sizing in this research work is more conservative compared to the pillar to diameter ratio of 1.8 reported in the previous studies [35] based on the salt fracture criterion.

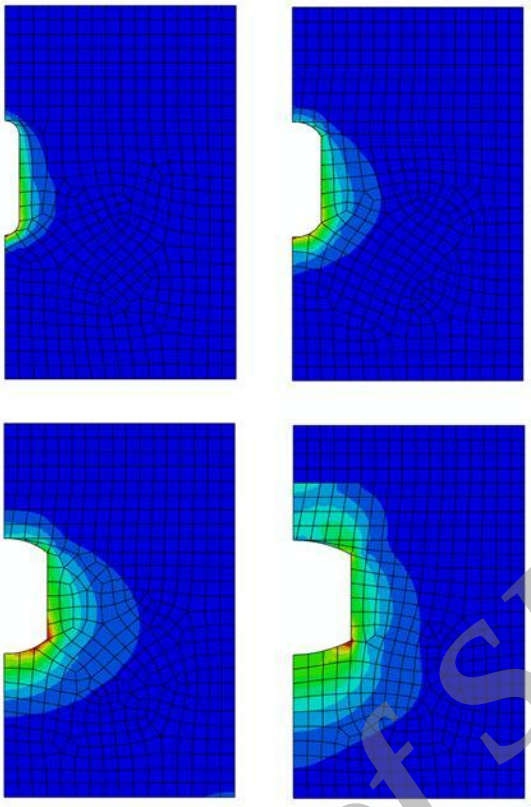

Figure 21. Equivalent Von Mises stress for caverns with diameters of 100, 200, 300, and 400 m.

In order to maintain the developed state of the stress in the cavern below the state of stress which causes the salt to dilate, the minimum and maximum gas pressure inside the cavern should also be determined. It has been recommended that the cavern is not maintained at the minimum pressure for an extended time [20]. The minimum operating pressure gradient is recommended to be 0.15-0.25 psi/foot, starting at the casing shoe above the roof of the cavern [25]. The maximum cavern pressure is suggested to be 0.75-0.8 psi/foot [25]. The gas pressure in the developed models in this study was considered to be 6 MPa, which is close to the maximum suggested pressure. Based on these recommendations and the cavern depth in this study, the proper pressure range is 1.35-7.25 MPa. In order to investigate the above pressure range for the cavern under scrutiny in this study, the cavern with the diameter of 300 m is modeled with the pressure levels of 1, 5, and 8.5 MPa. The values for the principal stress and stress invariants are calculated for the pressure scenarios, and plotted in Figure 22. The 1 MPa pressure causes the dilatancy and micro-fracture of the salt near the cavern, and the state of stress for 8.5 MPa is also very close to the dilatancy envelope. The 5 MPa state is far away from the envelope, and is considered as a safe state of stress. Also it was concluded that the minimum gas pressure is more prone to the dilatancy compared to the maximum gas pressure after 5 years. The FEM study for the caverns with other diameters delivers the same results. Therefore, the minimum and maximum operating pressures can be considered as 1.35 and 7.25 MPa, respectively.

In this research work, the results of the experimental set up (multi-stage creep tests) were implemented in the power law creep model of the FEM model to study the quasi-static creep behavior of the salt cavern in a long time period in order to investigate the stability of the cavern under different design-working scenarios, and to analyze the cavern closure. Also the experimental results of the multi-stage creep (stress invariants of the deviatoric stress tensor) were used to develop a dilatancy criterion, which was used to interpret the results of the numerical model for the stability of the cavern. The pillar size, operating pressure, and cavern diameter design guidelines were proposed based on the experimental and numerical models.

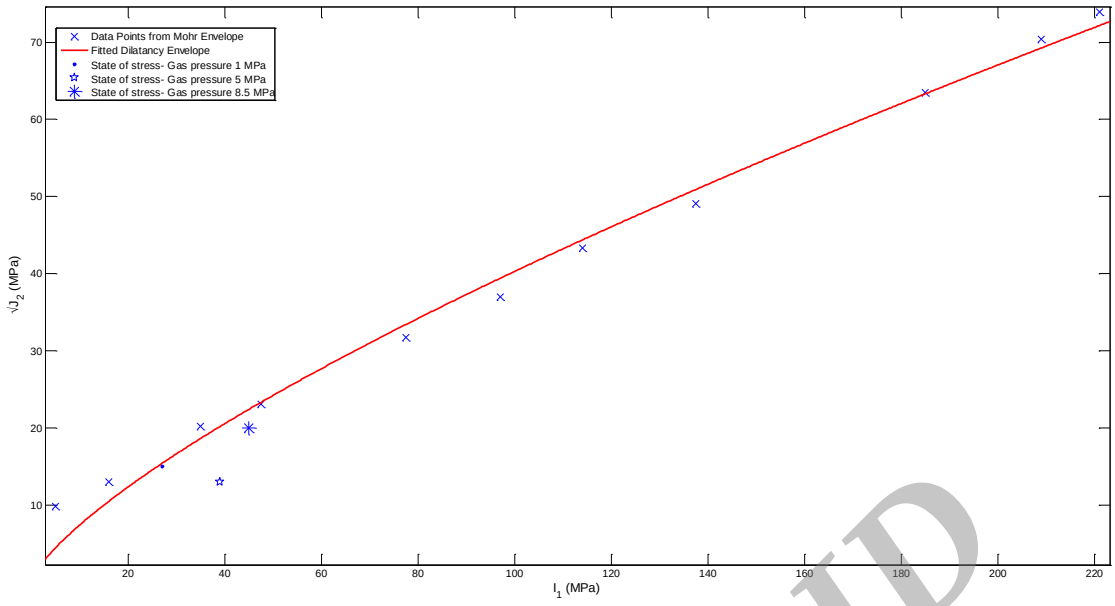

Figure 22. State of stress in dilatancy envelope for cavern with d=300 m and gas pressures of 1, 5, and 8.5 MPa.

6. Conclusions

The Fischells Brook salt deposit contains salt, making it suitable for the underground gas, compressed air, and liquid waste storage. In order to develop underground caverns, the geo-mechanics issues of the salt rock must be investigated to safely design the cavern. The steady-state creep behavior of the salt rock in underground caverns is one of the key engineering behaviors that causes the micro-fracture and closure of the cavern. The stability of the cavern under creep is dependent on some parameters such as the cavern size, operating pressure, and pillar sizing. Numerical modeling is the most efficient method to investigate the ideal size and operating conditions of the salt cavern. An empirical creep model was required for the numerical analysis of the cavern. A laboratory set up for the multi-stage constant stress creep was developed in this study to investigate the coefficients of the power law creep model and the strain rates of the core samples drilled in the Fischells Brook basin. Then an FEM model was developed to study the quasi-static creep behavior and closure of the cavern over a 5-year period. A dilatancy failure envelope was also developed to evaluate the stability of the cavern under the developed state of stress. The dilatancy criterion is based on the stress invariants of the deviatoric stress tensor, which determines the dilatant state of stress. Different scenarios for the cavern aspect ratio and the operating pressure were assumed for the sensitivity analyses. The deformation behavior and the developed state of stress were investigated for each scenario, and the results obtained were compared with the dilatancy envelope to determine the stability of the cavern. It was concluded that the closure and the affected stress area increase with increase in the cavern diameter. A pillar size and gas operating pressure range was also suggested.

Acknowledgements

The authors would like to acknowledge GeoStorage Associates of Nova Scotia for providing permission to publish the data and analysis of this work.

References

[1]. Hudson, J.A. (1993). Stability classes. In: J. A. Hudson (Eds.), Comprehensive Rock Engineering: Pergamon Press., Oxford, pp. 119-149.

[2]. Van Sambeek, L.L., Ratigan, J.L. and Hansen, F. D. (1993). Dilatancy of rock salt in laboratory test. International Journal of Rock Mechanics and Mining Science and Geomechanics Abstract. 30 (7): 735-738.

[3]. Thoms, R.L., Gehle, R.M. and Brassow, C.L. (1999). Analyses of salt caverns with granular wastes. Solution Mining Research Institute Spring Meeting, Las Vegas, NV, 11-14 April.

[4]. Chabannes, C.C, Durup, J.G. and Lanham, P. (1999). Geomechanical evaluation of Ssabine gas transmission company's cavern No. 2 at Spindel Top Salt Dome. Solution Mining Research Institute Spring Meeting, Las Vegas, NV, 11-14 April.

[5]. Ehgartner B. and Sobolik, S. (2002). 3-D cavern enlargement analyses (Tech. Rep. No SAND2002-

0526). Albuquerque, New Mexico: Sandia National Laboratories.

[6]. Nieland, J.D., Mellegar, K.D., Schalge, R.S. and Kaiser, H.D. (2001). Storage of chilled natural gas in bedded salt storage caverns (Tech. Rep. No DE-AC26-97FT34350). Huston, Texas: National Energy Technology Laboratory.

[7]. Fjaer, E., Holt, R.M., Horsrud, P., Raeen, A.M. and Risnes, R. (2008). Petroleum related rock mechanics (2nd. ed.), Elsevier, The Netherlands.

[8]. Cristescu, N. and Hunsche, U. (1992). Determination of nonassociated constitutive equation of rock salt from experiments. In: D. Besdo & E. stein (Eds.), IUTAM Symposium. Springer, Hannover, Germany, 511-523.

[9]. Jin, J. and Cristescu, N.D. (1998). An elastic/viscoplastic model for transient creep of rock salt. International Journal of Plasticity. 14 (1-3): 85-107.

[10]. Cristescu, N. (1993). A general constitutive equation for transient and stationary creep of rock salt. International Journal of Rock Mechanics and Mining Science and Geomechanics Abstract. 30: 125-140.

[11]. Hampel, A. and Schulze, O. (2007). The composite dilatancy model: A constitutive model for the mechanical behavior of rock salt. In M. Wallner, K. H. Lux, W. Minkey & H. R. Hardy (Eds.), 6th Conference on the Mechanical Behavior of Salt. Taylor & Francis, London, UK, 99-107.

[12]. Macky, F., Inoue, N., Fontoura, S.A.B. and Botelho, F. (2008). Geomechanical effects of a 3D vertical salt well drilling by FEA. 42nd US Rock Mechanics Symposium, San Francisco, CA, 29 June- 2 July.

[13]. Carter, N.L., Hanin, J., Russell, J.E. and Horseman, S.T. (1993). Rheology of rocksalt. Journal of Structural Geology, 15(9/10): 1257-1271.

[14]. Frayne, M.A., Rothenburg, L. and Dusseault, M.B. (1993). Four case studies in saltrock-Determination of material parameters for numerical modeling. In Mechanical Behavior of Salt, Proceeding of the Third Conference on Mechanical Behavior of Salt. Paris, France, 457-468.

[15]. Bar-Cohen, Y. and Zacny, K. (2009). Drilling in extreme environments: Penetration and sampling on earth and other planets. Wiley, Weinheim, Germany.

[16]. Chan, K., Bodner, S., Fossum, A. and Munson, D. (1997). A damage mechanics treatment of creep failure in rock salt. International Journal of Damage Mechanics. 6: 121-152.

[17]. Spiers, C.J., Peach, C.J., Brzesowsky, R.H., Schutjens, P.M.T.M., Liezenberg, J.L. and Zwart, H.J. (1988). Long term rheological and transport properties of dry and wet salt rocks (Tech. Rep. No FI1W-0051-NL), Brussels, Belgium: Commission of the European Committees.

[18]. Ratigan, J.L., Van Sambeek, L.L., DeVries, K.L. and Nielan, J.L. (1991). The influence of seal design on the development of the disturbed rock zone in the WIPP alcove seal tests (Tech. Rep. No RSI-0400). Albuquerque, New Mexico: Sandia National Laboratories.

[19]. Hunsche, U.E. (1993). Failure behaviour of rock around underground cavities. 7th International Symposium on Salt, Kyoto, Japan, 6-9 April, 59-65.

[20]. DeVries, K.L., Mellegar, K.D., Callahan, G.D. and Goodman, W.M. (2005). Cavern roof stability for natural gas storage in bedded salt (Tech. Rep. No RSI-1829DE-FG26-02NT41651). Rapid City, Dakota: National Energy Technology Laboratory.

[21]. Schmidt, U. and Staudtmeister, K. (1989). Determining minimum permissible operating pressure for a cavern using the finite element method, storage of gases in rock caverns. In B. Nielsen & J. Olsen (Eds.), International Conference on Storage of Gases in Rock Caverns, Rotterdam, The Netherlands, 103-113.

[22]. Fokker, P.A., Kenter, C.J. and Rogaar, H.P. (1993). The effect of fluid pressures on the mechanical stability of (rock) salt. In H. R. Hardy, Jr., T. Hoshi & K. Toyokura (Eds.), 7th Symposium on Salt, Kyoto, Japan, 6-9 April, 75-82.

[23]. Cosenza, Ph. and Ghoreychi, M. (1999). Effect of very low permeability on the long-term evolution of a storage cavern in rock salt. International Journal of Rock Mechanics and Mining Science. 36(4): 527-533.

[24]. Hoffman, E.L. and Ehgartner, B.L. (1993). Evaluating the effects of number of caverns on the performance of underground oil storage facilities. 34th U.S. Symposium on Rock Mechanics (USRMS). Madison, Wisconsin, 28-30 June, 1-4.

[25]. Adams, J. (1997). Natural gas salt cavern storage operating pressure determination, Technical Meeting/Petroleum Conference of the South Saskatchewan Section, Regina, Saskatchewan, 19-22 October, 1-15.

[26]. Han, G., Bruno, M.S., Lao, K., Young, J. and Dorfmann, L. (2007). Gas storage and operations in single-bedded salt caverns: Stability analyses. SPE Production and Operations. 22 (03): 368-376.

[27]. Ardeshiri, S. and Yazani, M. (2008). Numerical study of fault geometrical effects on seismic stability of large underground caverns. 42nd U.S. Rock Mechanics Symposium (USRMS). San Francisco, CA, 29 June-2 July, 1-8.

[28]. Hilbert, L.B. and Exponent, V.K. (2008). Salt mechanics and casing deformation in solution-mined gas storage operations. 42nd U.S. Rock Mechanics Symposium (USRMS). San Francisco, CA, 29 June-2 July, 1-12.

[29]. Ma, H., Yang, C., Qi, Z., Li, Y. and Hao, R. (2012). Experimental and Numerical analysis of salt cavern convergence in ultra-deep bedded formation. 46th U.S. Rock Mechanics/Geomechanics Symposium. Chicago, IL, 24-27 June, 1-8.

[30]. Nazary Moghadam, S., Mirzabozorg, H. and Noorzad, A. (2013). Modeling time-dependent behavior of gas caverns in rock salt considering creep, dilatancy and failure. Tunneling and Underground Space Technology. 33: 171-185.

[31]. Foster, S.J. and Halabura, S. (2008). Preliminary assessment study of potash resource prospectively, universal uranium exploration licences, Bay St. Georges subbasin, western Newfoundland, North Rim Exploration Ltd., Saskatoon, SK, Canada.

[32]. ASTM Standard D7070-08, (2008). Standard test methods for creep of rock core under constant stress and temperature. ASTM International, West Conshohocken, PA, www.astm.org.

[33]. ASTM Standard D4543-08, (2008), Standard practice for preparing rock core specimens and determining dimensional and shape tolerances. ASTM International, West Conshohocken, PA, www.astm.org.

[34]. Fossum, A.F. and Fredrich, J.T. (2002). Salt mechanics primer for near-salt and sub-salt deepwater Gulf of Mexico field developments (Tech. Rep. No SAND2002-2063), Albuquerque, New Mexico: Sandia National Laboratories.

[35]. Preece, D.S. and Wawersik, W.R. (1984). Leached salt cavern design using a fracture criterion for rock salt, 25th U.S. Symposium on Rock Mechanics (USRMS), Evanston, IL, 25-27 June, 1-10.

امکان‌سنجی مهندسی مخازن زیرزمینی در بسترهای نمکی غرب نیوفاندلند: بررسی آزمایشگاهی و اجزا محدود پایداری ناشی از خزش

احمد قاسملونیا [1*] و Stephen Butt [2]

۱- محقق پسا دکتری، ساب سورفیس ایمجینگ تکنولوژی، سنت جانز، نیوفاندلند، کانادا

2. Professor, Faculty of Engineering, Memorial University, St. John's, Newfoundland, Canada

ارسال ۲۰۱۴/۱۰/۲۰، پذیرش ۲۰۱۵/۶/۶

* نویسنده مسئول مکاتبات: a.ghasemloonia@mun.ca

چکیده:

استفاده از مخازن زیرزمینی در بسترهای نمکی مطمئن‌ترین روش دفن زباله‌های اتمی و ذخیره گاز است. ذخیره‌سازی گاز نقشی حیاتی را در روابط استراتژیک بین منابع بالادستی انرژی و کمپانی‌های مصرف‌کننده انرژی بازی می‌کند. منطقه فیشل بروک یک منطقه بالشتی شکل نمکی در ناحیه سنت جورج و در جنوب غرب نیوفاندلند قرار دارد و با دارا بودن سه بستر نمکی، پتانسیل حفر مخازن زیرزمینی برای ذخیره‌سازی گاز را داراست. توسعه این مخازن زیرزمینی نیاز به مطالعات پایداری از طریق آنالیزهای عددی و آزمایشگاهی دارد. این مطالعه تحقیقاتی با هدف بررسی امکان‌سنجی مهندسی مخازن زیرزمینی در این منطقه و بررسی پایداری این مخازن انجام‌شده است. در این تحقیق، تجهیزات آزمایشگاهی برای تعیین ضرایب مشخصه خزش سنگ نمکی ساخته شد. سپس این ضرایب مشخصه در مطالعات اجزا محدود استفاده‌شد تا آنالیز پایداری مخازن زیرزمینی نیوفاندلند در یک دوره پنج‌ساله بررسی شود. برای بررسی و تفسیر نتایج به‌دست‌آمده از روش اجزا محدود در این مطالعه، یک منحنی اتساع بر پایه تنش ارائه‌شده است که آنالیزهای حساسیت برای سناریوهای مختلف طراحی این مخازن زیرزمینی نیز بر اساس این منحنی تفسیر می‌شود. پیشنهادهای طراحی مهندسی ارائه‌شده در این تحقیق به‌عنوان یکی از بخش‌های کلیدی طراحی مهندسی در مخازن زیرزمینی بسترهای نمکی در نیوفاندلند استفاده خواهد شد.

کلمات کلیدی: مخازن زیرزمینی، بسترهای نمکی، مدل‌های خزش، منحنی اتساع شکست، مطالعات اجزا محدود، تست خزش تک‌محوری، پایداری مخزن زیرزمینی.